Journal of Polymer Research (2022) 29: 304
https://doi.org/10.1007/s10965-022-03159-3

ORIGINAL PAPER

Synthesis, optical and dielectric properties of polyacryloyloxy imino fluorophenyl acetamide and polyacryloyloxy imino fluorophenyl acetamide-co-polystyrene sulfonate

Rasha A. Baseer[1] · **Ewies F. Ewies**[2] · **A. M. Ismail**[3]

Received: 12 January 2022 / Accepted: 21 June 2022 / Published online: 30 June 2022

Abstract

Our scope is synthesis a new poly fluorobenzamide oxime ester and study its structural, optical, and dielectric properties. Consequently, ((*E*)-2-((acryloyloxy)imino)-*N*-(4-fluorophenyl) acetamide) (**AIFPA**) was as-synthesized via a condensation reaction of (*E*)-*N*-(4-fluorophenyl)-2-(hydroxyimino) acetamide with acrylic acid to polymerize it via free radical polymerization (**PAIFPA**). over and above, the synthesized PAIFPA was inserted in more polymerization action with polystyrene sulfonate through the grafting process (PAIFPA-co-PSS). The chemical structures and morphology of AIFPA, PAIFPA, and PAIFPA-co-PSS were characterized by 1H NMR, FTIR, and XRD. The crystallinity index of PAIFPA, and PAIFPA-co-PSS was studied, affording that PAIFPA-co-PSS has the highest crystallinity. Moreover, The optical bandgap that obtained from absorbance analysis was encountered to be in the range of 2.6 eV to 3.5 eV. Ultimately, the dielectric properties of PAIFPA, and PAIFPA-co-PSS showed that electric conductivity values ranged from 6.12×10^{-8} to 7.11×10^{-7} S.cm^{-1}, and 5.48×10^{-10} to 7.75×10^{-8} S.cm^{-1}, respectively. It has a great deal of interest of PAIFPA-co-PSS which has wide band gap energy as short-wavelength light absorbers to be used in tandem polymer solar cells.

Keywords Polyoxime Ester · Polystyrene · Optical · Dielectric

Introduction

MacDiarmid and coworkers discovered the significant features of conjugated polyacetylene to be a conducting polymer in the last century, notably in 1976, and how to enhance its ability over the full range from insulator to metal [1].

✉ Rasha A. Baseer
ra.abdelbasser@nrc.sci.eg; rasha.daaader@gmail.com

Ewies F. Ewies
ewiesfawzy@yahoo.com; ef.ewies@nrc.sci.eg

A. M. Ismail
asmaanrc@yahoo.com

[1] Department of Polymers and Pigments technology, National Research Centre, 33 ElBohouth St., (Former El Tahrir) Dokki, P.O. 12622, Dokki- Giza, Egypt

[2] Organometallic and Organometalloid Chemistry Department, National Research Centre, 33 ElBohouth St., (Former El Tahrir) Dokki, P.O. 12622, Giza, Egypt

[3] Spectroscopy Department, National Research Centre, 33 ElBohouth St., (Former El Tahrir) Dokki, P.O. 12622, Giza, Egypt

In general, conjugated polymers have been described as an alternating single (σ-bond) and double (π-bond) bonds along the carbon atoms on the alternating units[2] such as polyaniline [3, 4], polyacetylene [5, 6], polyfuran [7], polystyrene [8, 9], and Poly(vinyl carbazole) [10]. The hybridization of the carbon atom in the π-bond is sp^2p_z which overlap over the polymer skeleton, allowing the electron mobilization and charge transfer. Okutan et al. [11] studied the Impedance spectroscopy of polyaniline as a conductive polymer coated hydrogel. Ahlatcıoğlu [10] investigated the electro-optical properties of nanoclay/ poly(N-vinyl carbazole) nanoclay composites. Wang et al. [12] prepared polyolefin (COC)/polystyrene vitrimers (PSVMs) to reduce e-waste environmental contamination by using recycled printed circuit boards.

The conjugated polymer's diverse applications in various technologies have recently received a lot of attention due to their ability to combine the unique properties of conventional polymers such as low weight, good mechanical and flexibility with those of conventional semiconductors such as light emission and absorption, and tunable conductivity.Conjugated polymers, for example, have been used in a variety of critical applications, including

electrods[13], solar cell [14, 15], optoelectronic devices [16–18], supercapacitor [19, 20], sensors [21, 22], smart fabrics [7, 23], transistors [24] and medical applications [25, 26].

Fluorination of the conjugated polymer skeleton has recently emerged as a promising method for improving the conjugated polymer's performance conductivity [27, 28]., fluorinated polymers are marked by high thermal resistance, besides their reactivity to different chemicals and good mechanical properties, which qualify them to be applied in membranes, coatings, and other applications [29–31].

On the other hand, Oxime is an organic group that belongs to imine with a general formula RR'C=N–OH with an organic side chain with hydrogen (R and R'). It is usually generated from carbonyl compounds with hydroxylamines via condensation. Also, oxime bonds are more stable than the corresponding hydrazone or imine at physiological pH, which is useful in biomedical applications [32]. Further, oxime is integrated in many industrial applications, such as Nylon 6 via synthesis of Caprolactam [33], as antidotes for nerve agents to treat organophosphorus poisonous [34], and commercial fragrances such as buccoxime and Stemone [35]. Also, owing to the properties of oxime bond formation, oxime chemistry is used for bioconjugation with only water as a side product [36, 37], and perillaldehyde is an artificial sweetener in Japan [38]. Oxime ligation has been utilized to functionalize polymers with micro and macromolecules of interest such as polycaprolactone [39], polyketoester [40], methacrylate [41], glycoproteins [42], bovine serum albumin, [43] vinyl levulinate [44]. As a matter of fact, oxime ester is less used in polymer applications. However recently, polyoxime ester has been used to enhance the performance of thermoset polymers [45, 46].

Styrene is a vital raw material in different industrial applications. Polystyrene sulfonate (PSS) has been widely used in a variety of applications over the last few decades, including electric devices as a hole transport material in polymer solar cells (PSCs) [15, 47], dye removal [48], polymer- stabilizer [49] and medical applications [50–52].

In this study, a new fluoro oxime ester ((*E*)-2-((acryloyloxy)imino)-*N*-(4-fluorophenyl) acetamide) (AIFPA) was synthesized by combining (*E*)-*N*-(4-fluorophenyl)-2-(hydroxyimino) acetamide with acrylic acid and polymerizing it via free radical polymerization (PAIFPA). Furthermore, the as-synthesized polymer has been incorporated into the grafting process with styrene sulfonate (PAIFPA-co-PSS). The chemical structures of fluoro oxime ester, PAIFPA, and PAIFPA-co-PSS were approved with FTIR and 1H NMR analysis. The molecular weight of both PAIFPA and PAIFPA-co-PSS was studied using 1H NMR analysis. Eventually, dielectric studies and optical properties have been explored for PAIFPA and PAIFPA-co-PSS.

Experimental and methods

Materials

4-fluoroaniline and chloral hydrate (Oxford Laboratory), sodium sulfate and hydroxylamine (Merc), benzoyl peroxide and polystyrene sod.sulfonate (Modern Lab chemicals, Egypt), chloroform (Sigma), HCl (Elnasr Co., Egypt).

Measurement techniques:

The 1H NMR spectra were performed using a Bruker Advance II 400 MHz spectrometer using deuterated dimethylsulfoxide as the solvent. The XRD has been performed via PANalytical X'Pert Pro with Cu-Kα radiation (λ=0.154060 nm) at 30 kV and 30 mA. The patterns have been collected within the Bragg's angle (2θ) ranging between 10° and 80°. FTIR-ATR spectral data was collected in the range of 4000–400 cm^{-1} using the spectrometer VERTEX 80 (Bruker Corporation, Germany). Ultraviolet–visible absorption spectra were measured using Jasco V-630 UV–VIS (Japan) in the wave length region of 200–1000 nm. Investigations on the samples dielectric properties were carried out at room temperature utilizing a Novocontrol high-resolution alpha analyzer over the frequency range of 10^{-1}–10^{7} Hz. In order to create a parallel-plate capacitor cell, the studied samples, each having a thickness that ranged from 1 to 2 mm, were sandwiched between two freshly polished brass electrodes that had a top electrode diameter of 10 mm like (Scheme 1). The complex permittivity, denoted by the equation $\varepsilon^*=\varepsilon'-i\varepsilon''$, was determined by applying a sinusoidal voltage with an amplitude of 1 V to a frequency range covering 10^{-1}–10^{7} Hz. The examined composites can be characterized for complex dielectric spectroscopy by any of the complex parameters that are connected to each other by the equation that is presented below.

$$\varepsilon^*(\omega) = \varepsilon'(\omega) - i\varepsilon''(\omega) = \frac{1}{M^*} = \frac{\sigma^*}{i\omega\varepsilon_o} \quad (1)$$

where M* is the complex dielectric modulus, σ* is the complex electric conductivity, ω is the angular frequency and ε_o is the vacuum permittivity (see Scheme 2).

Methods

(*E*)-*N*-(4-fluorophenyl)-2-(hydroxyimino)acetamide synthesis

At 50 °C, 4-fluoroaniline (74 mmol, 4 mL) was dissolved dropwise (using a 1 mL syringe for addition) in 250 mL of 0.1 M HCl solution. Then hydroxylamine HCl (259 mmol, 9.5 g) followed by sodium sulfate (600 mmol, 42 g) were added. Chloral hydrate (88.8 mmol, 7.6 g) was dissolved in the solution, which was then stirred overnight at 50 ± 5 °C. The suspension was

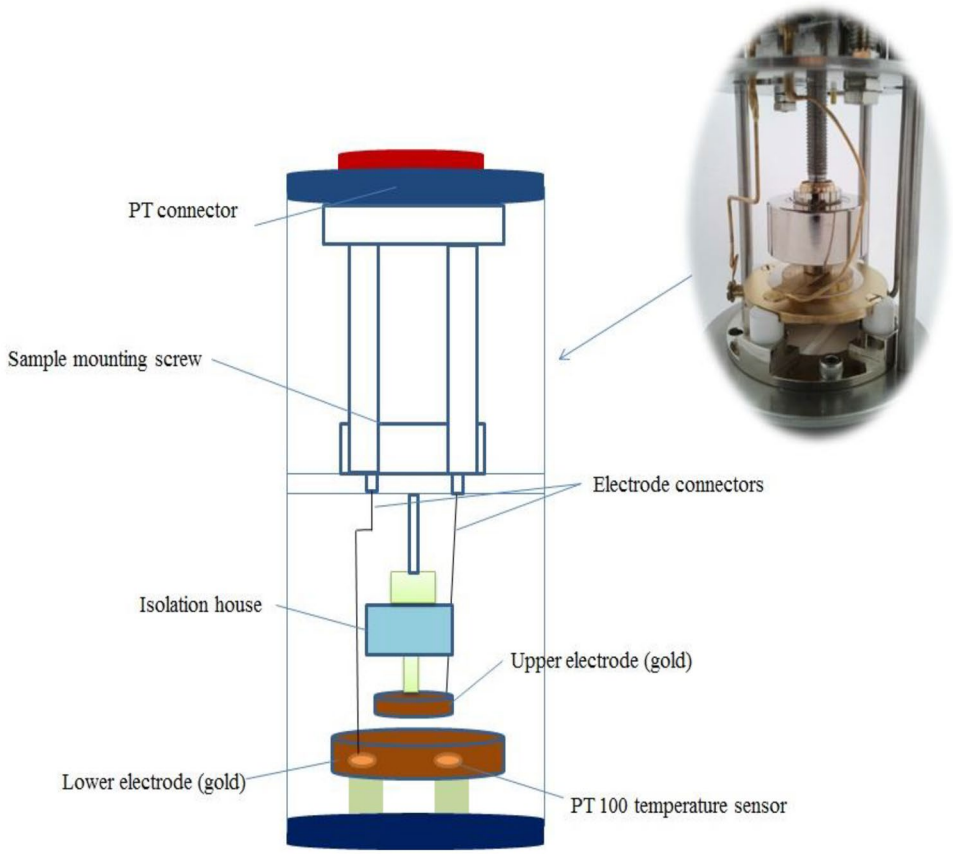

Scheme 1 Schematic illustration of electrical measurement

filtered and the filtrate discarded. The solid was washed with water and allowed to air dry for at least 24 h [53].

(*E*)-2-((acryloyloxy)imino)-*N*-(4-fluorophenyl)acetamide synthesis (AIFPA)

1 mol of (*E*)-N-(4-fluorophenyl)-2-(hydroxyimino) acetamide was condensed with 1 mol of acrylic acid at 60 5 C for 2 h while stirring. Brownish sticky amidoester was obtained and confirmed using TLC, then measured qualitatively.

Poly((*E*)-2-((acryloyloxy)imino)-*N*-(4-fluorophenyl) acetamide) synthesis (PAIFPA)

PAIFPA was synthesized via free radical polymerization. Where, 0.2 g of benzoyl peroxide was added to a preweighed amount of AIFPA dissolved in 20 mL of DMF and refluxed at 80 ± 5 ˚C, stirring for 5 h. Eventually, the net product was washed several times with chloroform and dried in a vacuum furnace at 100 ˚C for 24 h.

Poly((*E*)-2-((acryloyloxy)imino)-*N*-(4-fluorophenyl) acetamide)-co-polystyrene sulfonate synthesis (PAIFPA-co-PSS)

In a round flask; 0.2 g of benzoyl peroxide (BPO) was added to a preweighed amount of PAIFPA dissolved in DMF, then 2 g of polystyrene sulfonate was added. The reaction vessel was allowed to reflux at 70 ± 5 ˚C for 5 h with stirring. The net product was washed several times with chloroform and dried in a vacuum furnace at 100 ˚C for 24 h (see Fig. 1).

Results and discussion

Synthesis of AIFPA

Herein, AIFPA was synthesized by reacting (*E*)-*N*-(4-fluorophenyl)-2-(hydroxyimino)acetamide with acryloyl group as shown in Scheme 3. Acryloyl groups are an enaone form with acrylic groups as α,β–unsaturated carbonyl moiety with a C = C double bond at which electrophilic addition

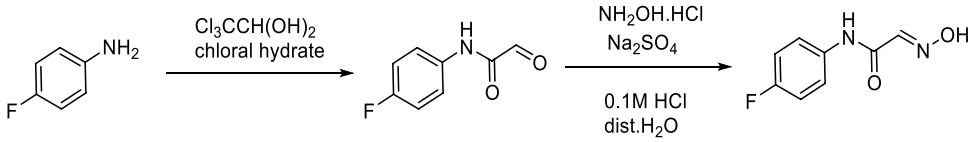

Scheme 2 (*E*)-*N*-(4-fluorophenyl)-2-(hydroxyimino) acetamide synthesis

occurs, at C = O; nucleophilic addition and substitution occur. The carboxylic group reacts with alcohol, oxime, ammonia,.....etc. and it has a conjugated double bond [54]. Acrylic polymer is also used in nail polish [55], as capping agents [56], and as polymer electrolyte in dye-sensitized solar cells (DSSCs).

Scheme 3 represents AIFPA synthesis, where its chemical structure is recogenized by 1H NMR (Fig. 2a), which shows (DMSO-d6) δ/ppm: 7.98 (s, NH amide), 7.90 (s, CH aldimine), 7.18–7.51 (m, 4H benzene), 6.43 (s, H 1-ethylene trans), 6.62 (s, H 1-ethylene cis), 6.49 (s, H 1-ethylene gem); IR cm^{-1} (Fig. 2) shows ν: 3133 (C = CH alkene, stretch for sp^2 carbon), 3013 (NH, stretch), 1764 (C = O, stretch), 1656 (-C = C- alkene, stretch), 1554 (NO, stretch), 1218 (C-O, ester, stretch), 989 (-CH bending R-CH = CH_2), 805 (*p*-subst. benzene). The fragmentation pattern of AIFPA is illustrated in Scheme 5 where, MS m/z: 236 (50%).

Synthesis of PAIFPA and PAIFPA-co-PSS

Scheme 4 demonstrates the predictable polymerization route of PAIFPA and PAIFPA-co-PSS via free radical generation using BPO.

1HNMR assured the chemical structure of the resulting PAIFPA and PAIFPA-co-PSS. Where, Fig. 2b represents 1HNMR of PAIFPA (DMSO-d_6) δ/ppm: 7.91 (s, NH amide), 7.66 (m, CH aldimine), 6.98–7.22 (m, 4H benzene), 6.78 (d, H 1-CC = O gem), 6.14 (d, H 1-CC = O cis), 2.95 (s, CH methine, 1 alpha –C = C), 2.82(s, CH methine, 1 alpha C), 2.42 (m, CH methine, 1 beta –C), 1.69 (m, CH_2 methylene), 1.06 (s, CH_3 methyl). On the other hand, Fig. 2c shows 1HNMR of PAIFPA-co-PSS (DMSO-d_6) δ/ppm: 7.98 (s, NH amide), 7.81–7.95 (m, 4H benzene of PSS), 7.56(m, CH aldimine), 7.41–7.49 (m, 4H benzene of PAIFPA), 7.18 (m, 1 -NC(= O)), 5.82 (m, H 1-CC = O cis), 3.3 (m, CH methine, 1 beta -C), 3.09 (m, CH methine, 1 beta -C), 2.83 (d, CH methine, 1 alpha –C = C), 2.57 (m, CH methine, 1 alpha C), 2.69 (m, CH methine, 1 alpha –C(= O)), 1.94 (td, CH_2 methylene), 1.23 (s, CH_3 methyl) (see Fig. 2).

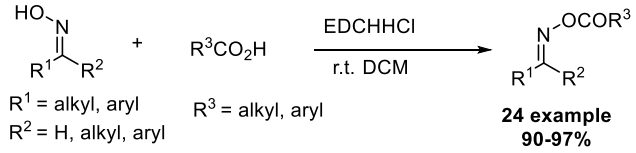

Fig. 1 ketoxime and aldoxime esters

Moreover, 1HNMR is a promising application for identifying molecular weight as the areas under resonance peaks match with the molar concentration of the moieties in the analyzed sample [57]. Josephat U. Izunobi and Clement L. Higginbotham conducted a comparative study of the polymer number-average molecular weight (Mn) for (MPEG-NH_2) and (MPEG-b-PLL(Z)) as model homopolymer and block copolymer, respectively using 1HNMR, GPC, and MALDI-TOFMS [58]. Mary L. Harrell and David E. Bergbreiter analyzed the number-average molecular weight of MPEG and its acetate derivative using 1HNMR.

The number of repeating unite (n) in each of PAIFPA, and PAIFPA-co-PSS has been calculated according to the following equation [58]

$$n_{x=\frac{a_x m_y n_y}{a_y m_x}} \quad (2)$$

where a_x is the area or intensity of the 1HNMR peak of moiety x; m_x is the number of protons of moiety x; a_y is the area or intensity of the 1HNMR peak of moiety y; n_y is the number of repeating units of moiety y; and m_y is the number of protons of moiety y.

$$n_{\mathrm{PAIFPA}=\frac{a_{CH} m_{CH3} n_{CH3}}{a_{CH3} m_{CH}}} \quad (3)$$

where a_{CH} is the sum of CH integerals

$$= \frac{(314.05 + 11.69) \times 3 \times 1}{55.02 \times 1} = 28.5 \approx 29$$

Hence; Mn of PAIFPA = 235.19 + (29 × 274) + 237.21 = 8418.4 ≈ 8418

$$n_{\mathrm{PAIFPA-co-PSS}=\frac{a_{CH} m_{CH3} n_{CH3}}{a_{CH3} m_{CH}}}$$

Scheme 3 (E)-2-((acryloyloxy) imino)-N-(4-fluorophenyl) acetamide synthesis

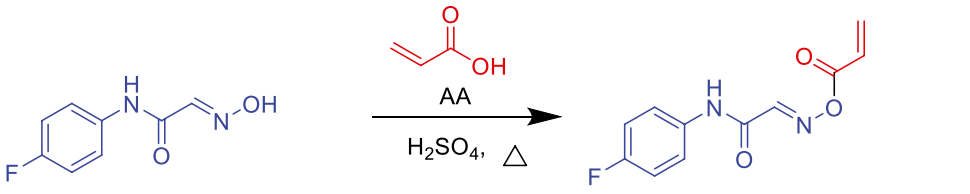

(*E*)-*N*-(4-fluorophenyl)-2-(hydroxyimino)acetamide

(E)-2-((acryloyloxy)imino)-N-(4-fluorophenyl)acetamide

AIFPA

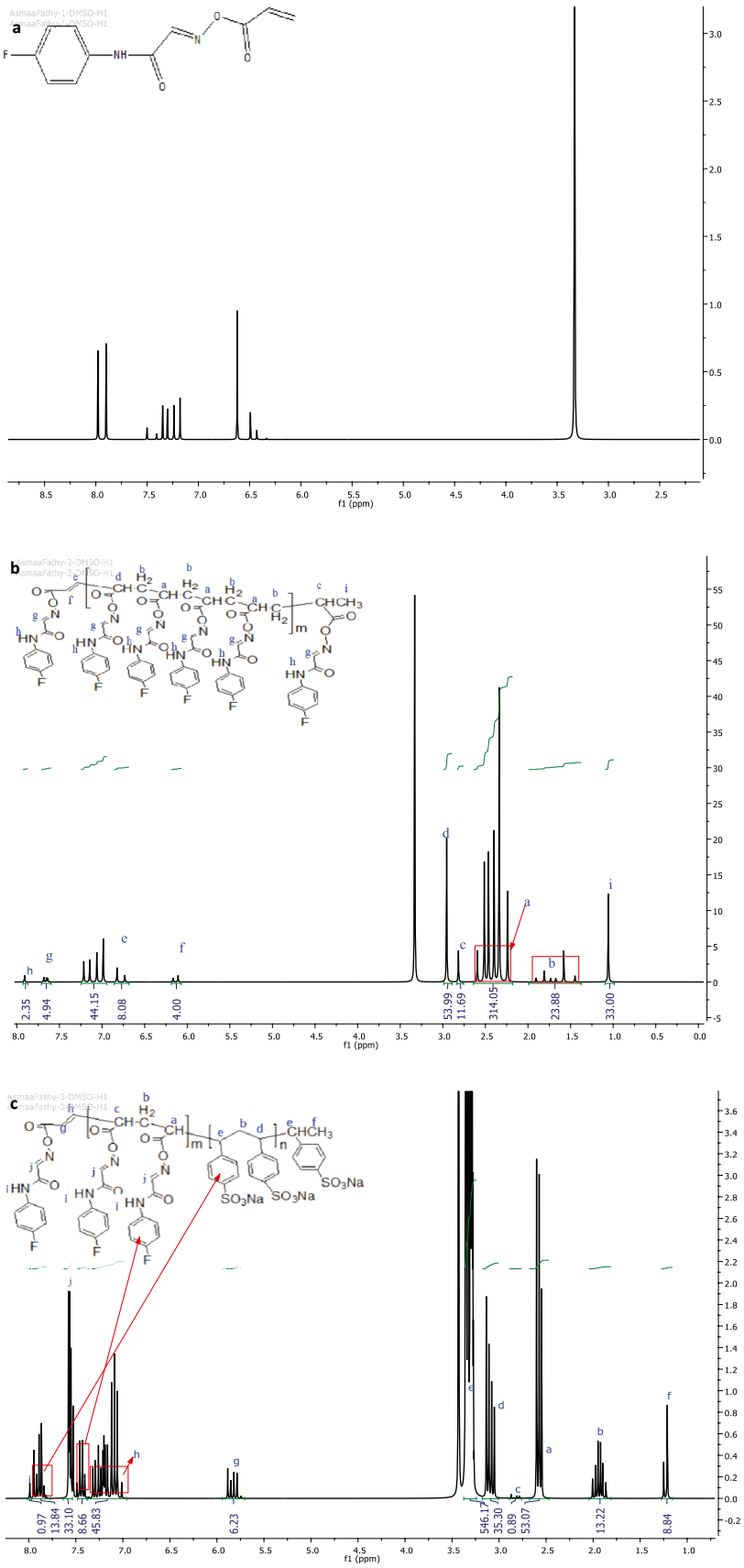

Fig. 2 1H NMR of: **a** AIFPA, **b** PAIFPA, and **c** PAIFPA-co-PSS

Where a_{CH} is the sum of CH integerals in PSS moiety

$$= \frac{(546.17 + 35.3) \times 3 \times 1}{8.84 \times 1} = 179.3 \approx 179$$

Hence; Mn of PAIFPA − co − PSS = 235.19 + (29× 274) + (179 × 193.18) + 207.2 = 42967.1 ≈ 42968

= 42967.1 ≈ 42968

Figure 3 shows the ATR-FTIR of PAIFPA, and PAIFPA-co-PSS. For PAIFPA, the weak band at 3084 cm^{-1} is assigned to C = CH stretching vibration, while the band at 2985 cm^{-1} is refered to N–H stretching vibration. Tt 2960 cm^{-1} and 2935 cm^{-1}, respectively asymmetric and symmetric stretching of CH_2 is observed [59]. The band at 1409 cm^{-1} for the C-H bending alkane methyle group. The strong band at 1160 for C-O ester stretching vibration. The band at 1714 cm^{-1} and 1602 cm^{-1} is attributed to C = O and C = N, respectively [60, 61]. The stretching vibration of C = C–C aromatic ring is assigned at 1508 cm^{-1} [62]. A band of amide II is seen at 1546 cm^{-1} [63]. The weak band at 1438 cm^{-1} corresponds to aromatic C–C bonds and C-H wagging [62, 64]. The bending vibration of aliphatic CH in methylene group is shown at 1397 cm^{-1} [65]. The stretching vibration of C-F is observed at 1324 cm^{-1} [66]. The stretching vibration of C-O is seen at 1166 cm^{-1}. The bending vibration of the monosubstituted alkene is presented at 989 cm^{-1}.The band at 836 cm^{-1} is assigned to

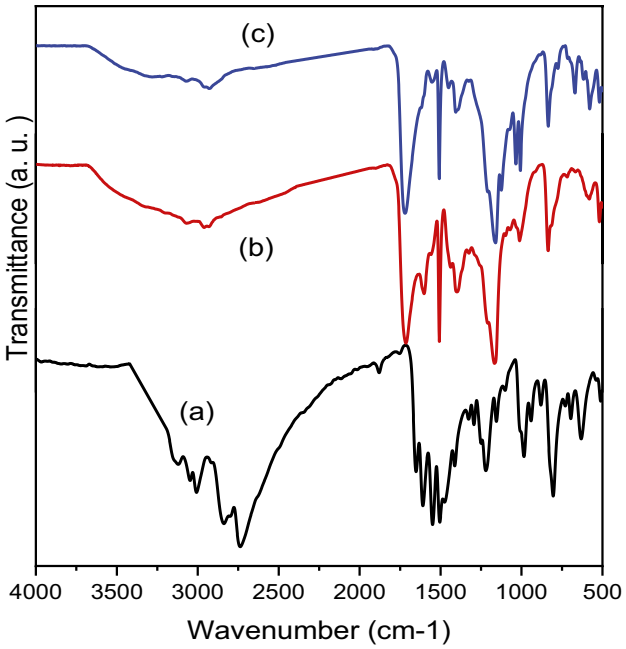

Fig. 3 ATR-FTIR of **a** AIFPA **b** PAIFPA, and **c** PAIFPA-co-PSS

the plane of aromatic C-H. C-H and C-F out of plane bending vibration is related to bands at 519 cm^{-1} and 499 cm^{-1} [66].

Bands at 1034 cm^{-1} and 1007 cm^{-1} correspond to asymmetric and symmetric stretching of S = O. A band at 670 cm^{-1}, which was attributed to the SO^{-3} group, confirmed the presence of PSS in the complex [67, 68]. These data indicate that the polymer consists of the SO^{-3} group and the complexation between fluorobenzene and sulphonated polystyrene.

ketoxime and aldoxime esters were synthesized in a very simple method by Kumar et al. [69] at which oxime reacted with acid in presence of a catalyst at room temperature.

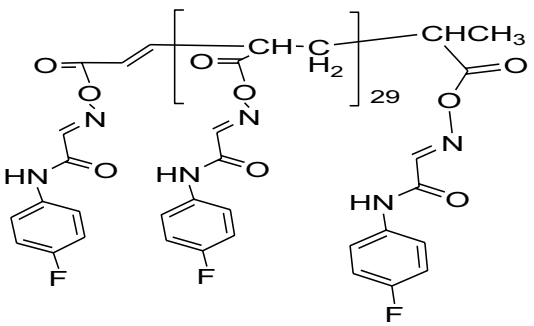

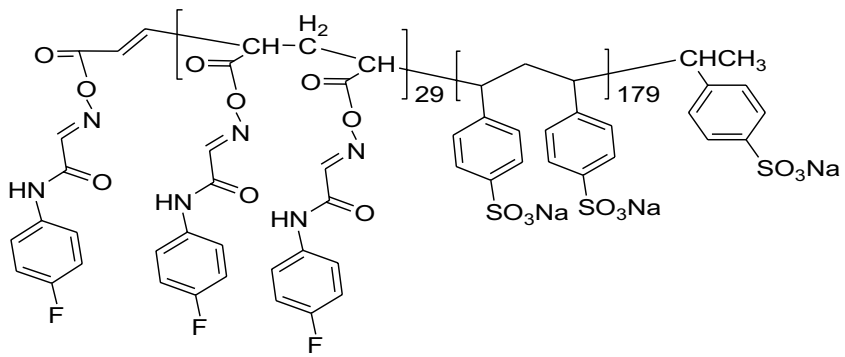

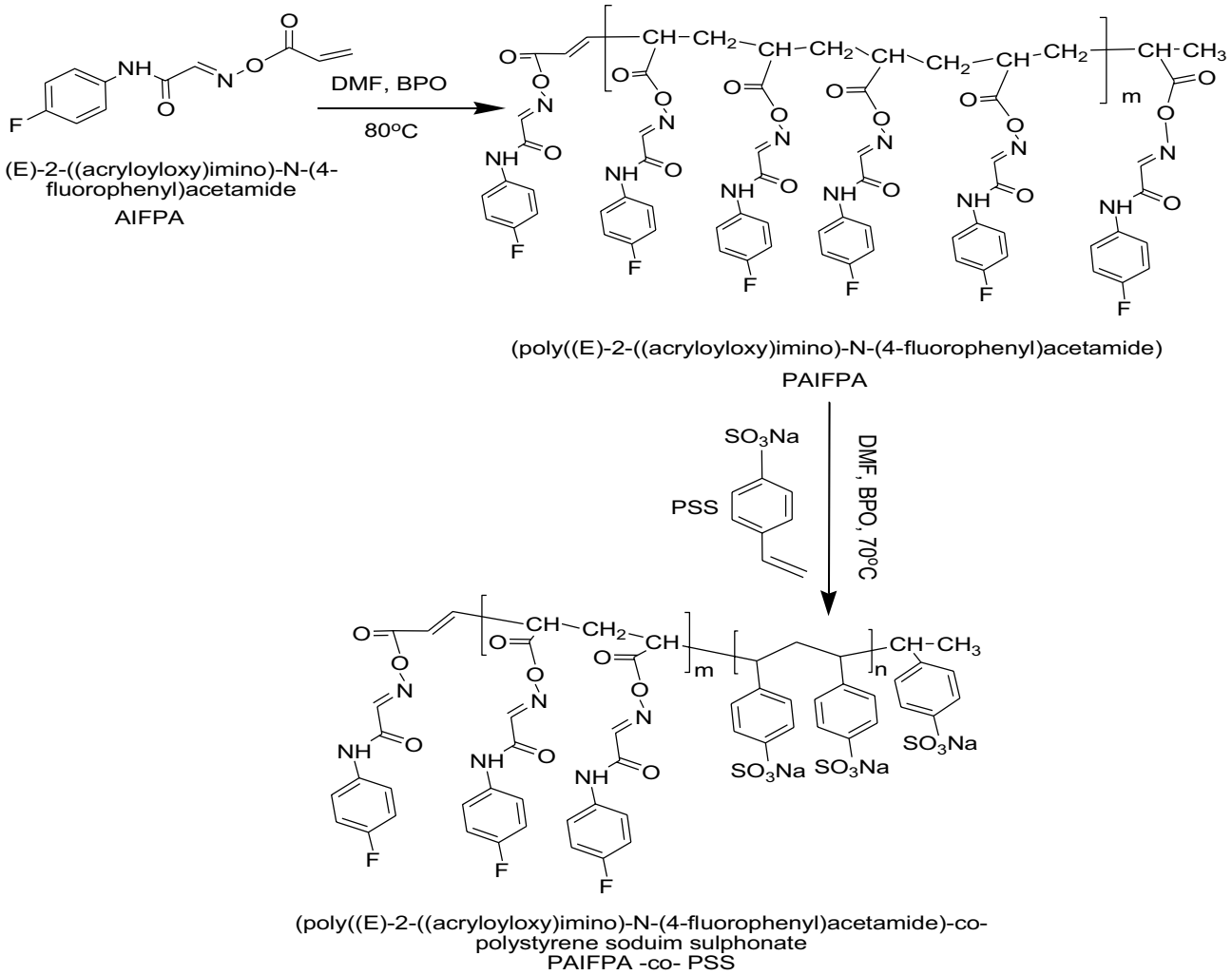

Scheme 4 Poly((E)-2-((acryloyloxy)imino)-N-(4-fluorophenyl)acetamide)-co-polystyrene sulfonate synthesis

X-ray Diffraction (XRD)

Figure 4 represents the XRD of PAIFPA, and PAIFPA-co-PSS. In contrast to the reality of fluorine atoms being macromolecule chain polarity booster leading to enhancing the crystallite regions by increasing the intermolecular forces, causing a higher crystallinity, PAIFPA has a broad single diffraction peak at $2\theta = 19.2°$ and virtually no crystal diffraction was witnessed. The observed amorphous diffraction may be induced because of the bulky fluorinated phenyl groups attached to the polymer skeleton, which generate looser chain packing and decrease the well-organized arrangement of the chain as well [70]. On the other hand, grafting PAIFPA with PSS enhances the crystallinity due to the existence of sulpher where a small peak is detected at $2\theta = 7.1°$ [48, 49]. Moreover, the presence of sulfonate ions increases intermolecular forces as the peak at $2\theta = 19.2°$becomes less broad and their intensity increases, and there are additional peaks appearing at $2\theta = 44.6°$ and 64.9° due to the electrostatic attraction between the negative charge of sulfonate ions and the positive charge generated on fluorine due to resonance as shown in Scheme 7. This means that the crystallinity increases and the interaction between PAIFPA and PSS.

The crystainaty indexs of both PAIFPA, and PAIFPA-co-PSS were calculated according to Eq. (1) [71]:

$$crystallinityindex\% = \frac{Intergratedareaofcrystainepeaks}{Totaintegeratedarea} \times 100 \quad (4)$$

where, the crystallinity indexs of PAIFPA, and PAIFPA-co-PSS were 36.23 and 77.99%, respectevily.

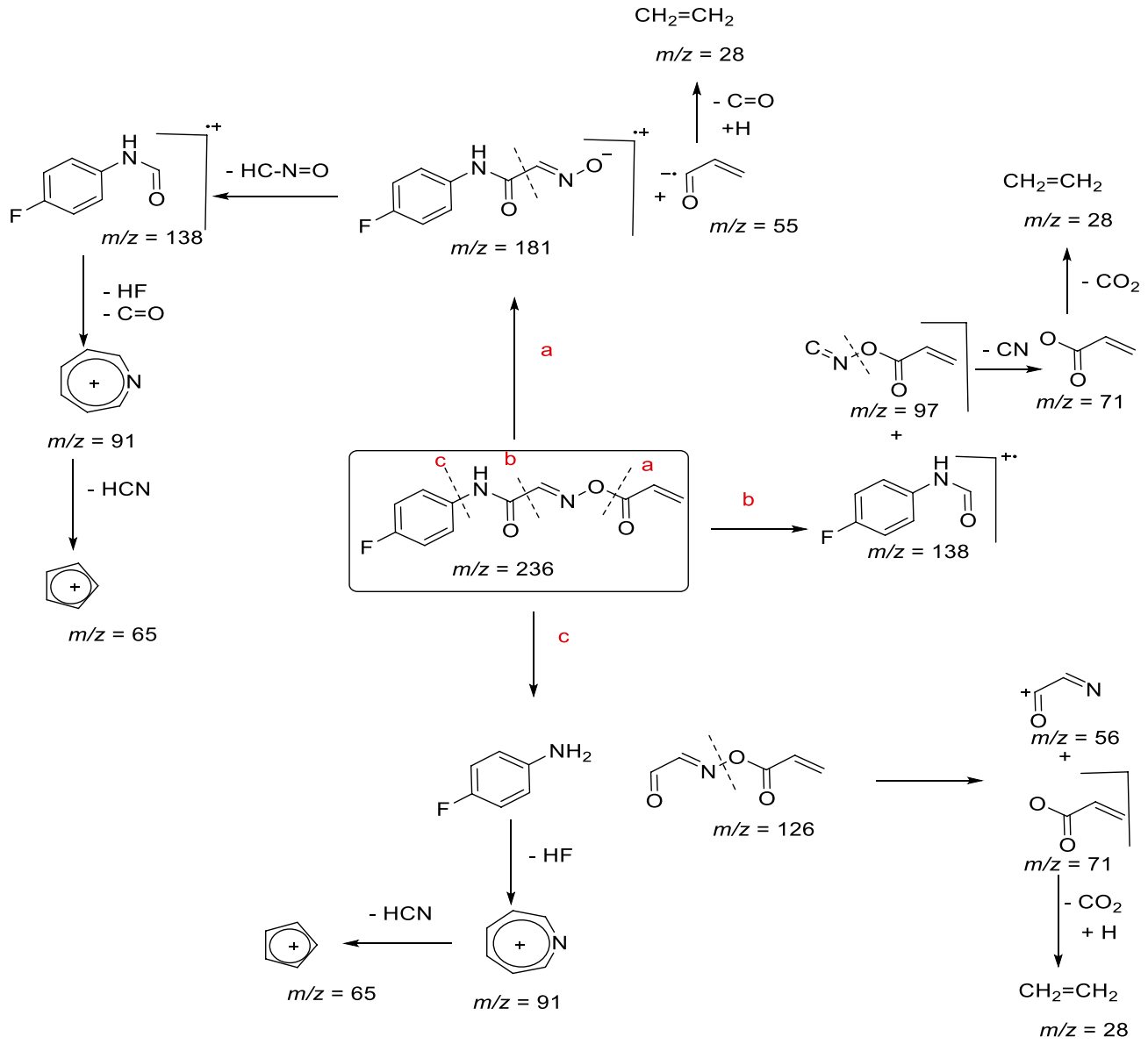

Scheme 5 fragmentation pattrern of AIFPA

Optical properties

Figure 5 shows the UV–Vis of PAIFPA, and PAIFPA-co-PSS. As seen in Fig. 5a, the two peaks, 208 nm and 232 nm, are assigned to n-π* and π-π* due to the presence of C=O, C=N, and C=C [72]. After the addition of PSS, the peaks at 208 nm and 232 nm are shifted to 204 nm and 226 nm (blue shift) (Fig. 5b) [68], which is matched with the fact of the electrostatic interaction between both fluorobenzene and sulfonated polystyrene.

The value of information obtained from the absorption coefficient (α), such as the optical band gap energy and the electronic band structure, is important for investigating the optical properties of a material. The absorption coefficient (α) is related to absorbance (A) and thickness of sample (d) according to the following [73]:

$$\alpha(\lambda) = \frac{2.303}{d}A \tag{5}$$

Figure 6 illustrates the relation between absorption coefficient (α) and photon energy (hυ). The extrapolation of the linear portion of the curve with zero values of photon energy gives the values of the absorption edge. As seen, the value of the absorption edge of PAIFPA-co-PSS is lower than its value in PAIFPA. This means that the reaction between PAIFPA and PSS reorders the atoms of the PAIFPA-co-PSS and increases its crystallinity, as confirmed by XRD.

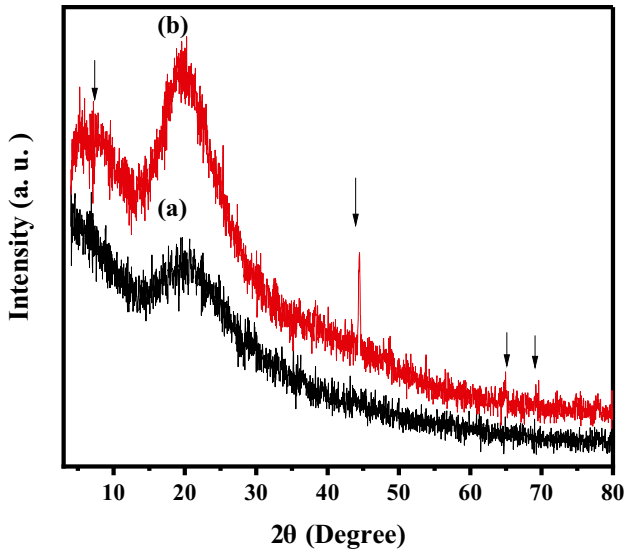

Fig. 4 XRD of (a) PAIFPA, and (b) PAIFPA-co-PSS

The optical transitions caused by photons of energy $h\upsilon > E_g$ can be investigated using the following relationship for near edge optical absorption [73].

$$\alpha h\upsilon = B(h\upsilon - E_g)^n \tag{6}$$

where B is constant, E_g is the band gap energy between valence and conduction band and n is called the power factor that characterize the optical transition. The power n takes value ½ for direct transition and 2 for indirect one.

The relation between $(\alpha h\upsilon)^2$ and $(\alpha h\upsilon)^{0.5}$ and $h\upsilon$ for PAIFPA, and PAIFPA-co-PSS is depicted in Fig. 7. As seen, the values of direct and indirect band gap energy for PAIFPA are lower than those for copolymer. This means

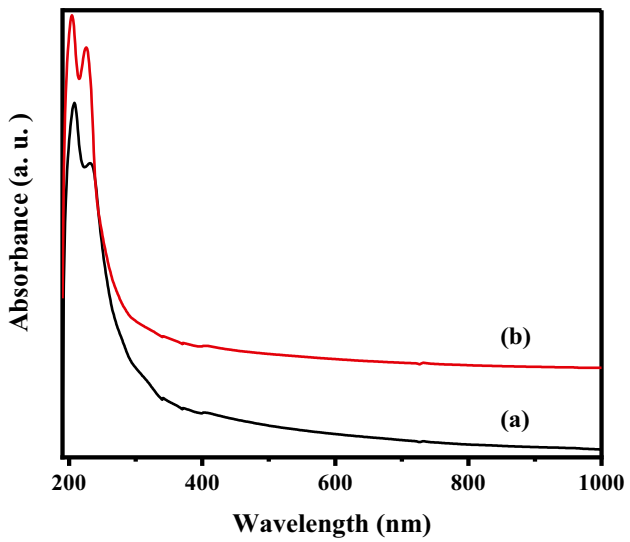

Fig. 5 UV–Vis spectra of **a** PAIFPA, and **b** PAIFPA-co-PSS

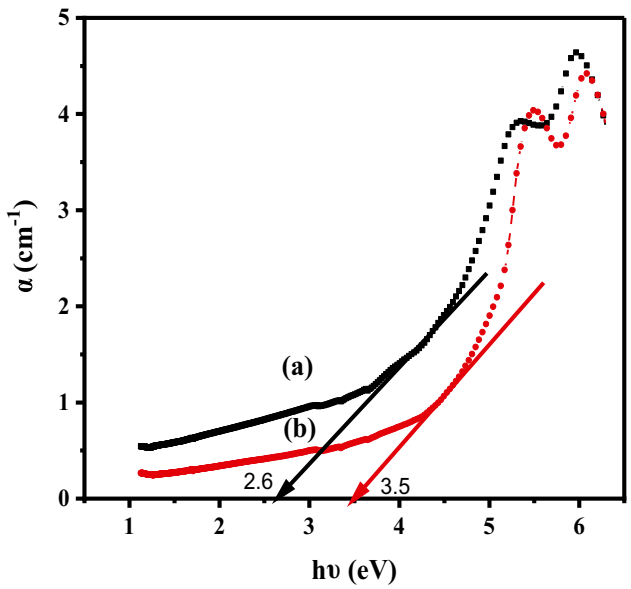

Fig. 6 Relation between absorption coefficient (α) and hυ of **a** PAIFPA, and **b** PAIFPA-co-PSS

that the addition of PSS to PAIFPA changes their electronic structure. The reaction between PSS and PAIFPA increases the gap that separates the two localized states in PAIFPA-co-PSS and increase the potential barrier between them. As a result, the transfer of charge carriers between the localized states becomes difficult.

When photon energy $h\upsilon < E_g$, the absorption of photons is associated to the existence of localized tail states in the forbidden gap that related to the amorphous nature of material. The width of this tail is known as the Urbach tail that indicates the defect levels in the forbidden band gap and calculated using the following formula [74].

$$\alpha = \alpha_0 \exp\left(\frac{h\upsilon}{E_u}\right) \tag{7}$$

where α_0 is a constant and E_u is the Urbach energy. Figure 8 illustrates the relation between ln α against hυ. The relation give straight line whose the reciprocal of this slope give the value of E_u. Values of band tail energy for PAIFPA is greater than that for PAIFPA-co-PSS which affirmed that the crystallinity is increasing by interacting PAIFPA with PSS.

Dielectric properties

The electronic structure of π-conjugated polymers is generated from the hybridized wavefunction (sp^2p_z) of the carbon atom of the repeat unite. Semiconducting polymers are recognized to possess energy bands generated from the σ-band and σ*-band energy levels related to the σ-bonds between adjacent carbon atoms (sp^2) which tighten the structure

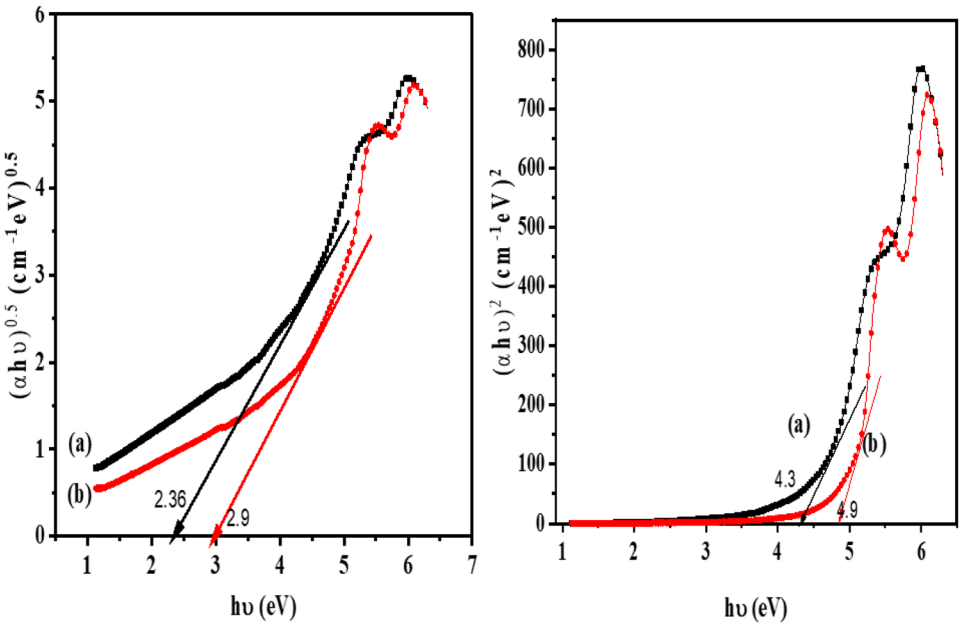

Fig. 7 Relation between $(\alpha h\upsilon)^{1/2}$ and $(\alpha h\upsilon)^2$ versus hυ for **a** PAIFPA, and **b** PAIFPA-co-PSS

together and the pz wavefunctions associated with π-bond which endow unique properties of the conjugated polymers as semiconductors [75]. The obtained results show electrical conductivity values for PAIFPA ranging from 6.12×10^{-8} to 7.11×10^{-7} S.cm^{-1} at low and high frequency, respectively. Scheme 6 illustrates the possible charge mobilization among the PAIFPA macromolecule structure under an electric field. The expected electron conjugation occurs across fluorobenzene to the amide moiety. And as is well known, fluorine is an electron-donating group by resonance (+M) creating a free electron radical cloud inside the benzene ring allowing reciprocal resonance in the benzene ring passing through the amide group which qualifies PAIFPA to be a p-type semiconducting polymer. On the other hand, contrary to expectations, electrical conductivity values of PAIFPA-co-PSS range from 5.48×10^{-10} to 7.75×10^{-8} S.cm^{-1} at low and high frequency, respectively, and this may back to the generated electrostatic attraction between fluorine and sulfonate ion leading to atom rearrangement and crystallinity increase as shown in XRD. In general and as is clear in Scheme 7, the sulfonate group is an electron- withdrawal group by resonance (–M) forming a hole (n-type) represented by a positive charge inside the benzene ring.

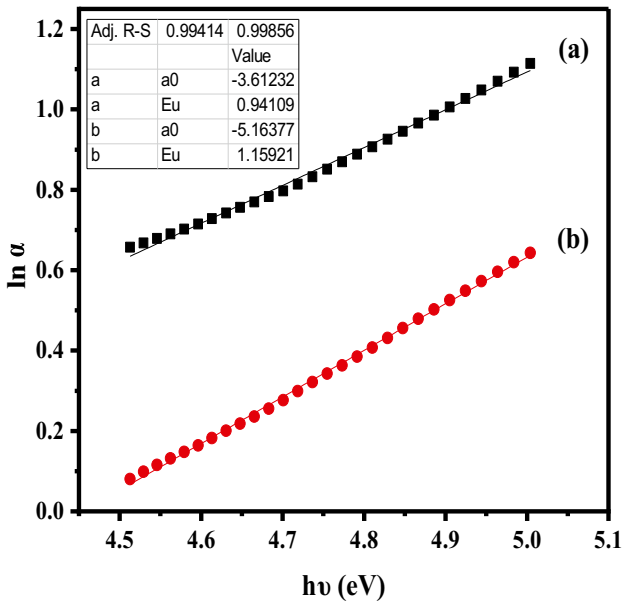

Fig. 8 Relation between ln (α) versus (hυ) for **a** PAIFPA, and **b** PAIFPA-co-PSS

It is possible to determine a material's ability to store electrical charges by evaluating their dielectric measurement. Figure 9 represents the relation between the logarithm of dielectric constant (ε') and dielectric loss (ε") against the logarithm of frequency (log f) for PAIFPA, and PAIFPA-co-PSS. This is due to the ability of dipoles in samples to align themselves in the field direction, as well as charge accumulation between electrodes.By increasing the frequency, the charge is unable to follow the rapid change in the electric field and " decreases. At higher frequencies than 100 kHz, however, the dielectric constant remains constant and is frequency independent. However, when the frequency decreases, the dielectric constant ε'rises. Because of interfacial space-charging polarization, it can be concluded that using thin insulation barriers does not completely prevent the accumulation of ionic charge at metallic electrodes/insulating barriers/ionic sample interfaces, as shown by the increase in ε' observed on low frequency plateaus. A

Scheme 6 Conjugation mechanism of PAIFPA

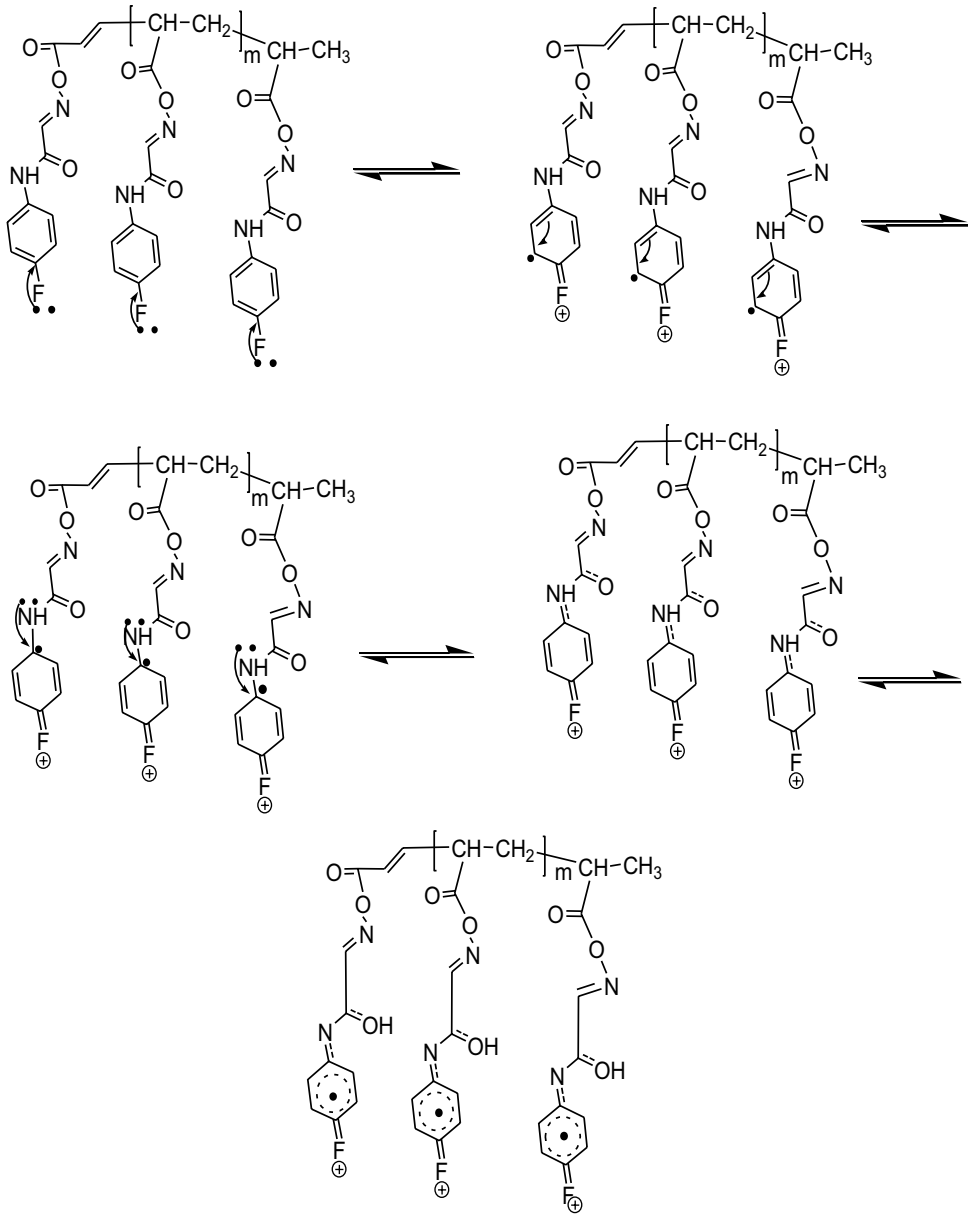

permanent dipole's alignment with the field and contribution to total polarization is complete at low frequencies [76]. As seen in Fig. 9, values of ε' and ε" for PAIFPA is higher than those for PAIFPA-co-PSS due to the addition of PSS restricting the motion of PAIFPA, so its values decrease [77].

The frequency dependence of conductivity is the summation of the amount of DC conductivity due to free charge movements and polarization conductivity due to bound charge movements. The increase in conductivity with frequency is popular for polymer and semiconductor materials. The first behaviour takes place when the frequency is independent of conductivity,which is contributed to by the free charges found in the material, and the second behaviour takes place when the frequency depends on the conductivity because of the trapped charge and it is only active in the high frequency region [78].

Figure 10 depicts the relationship between the logarithm of conductivity (log σ) as a function of the logarithm of frequency (log f). The increase in conductivity of all samples at high frequency because of the mobility of charge carriers is high in the high frequency field. As the frequency drops, more charge accumulates at the electrode–electrolyte interface, resulting in a reduction in the number of mobile ions and, finally, a decrease in conductivity at low frequencies [79].

The total conductivity, σ (ω) is the sum of dc and ac conductivity and is described using the following equation

Scheme 7 Conjugation mechanism of PAIFPA-co-PSS

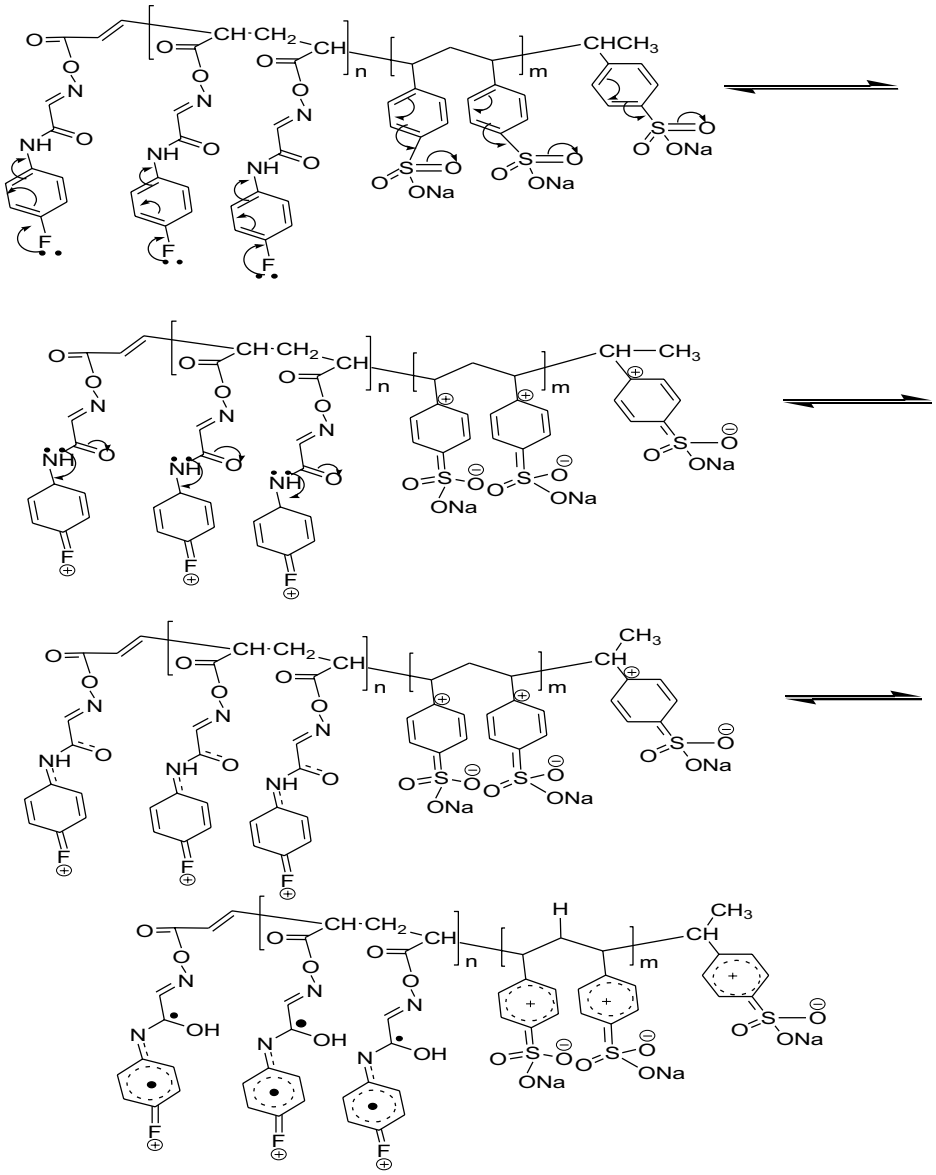

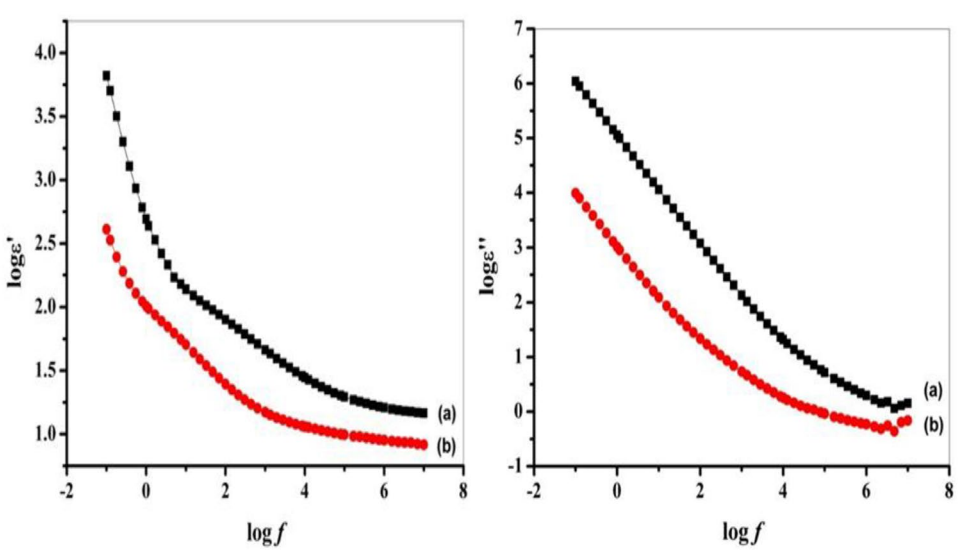

Fig. 9 Relation between log ε' and log ε" versus log f for **a** PAIFPA, and **b** PAIFPA-co-PSS

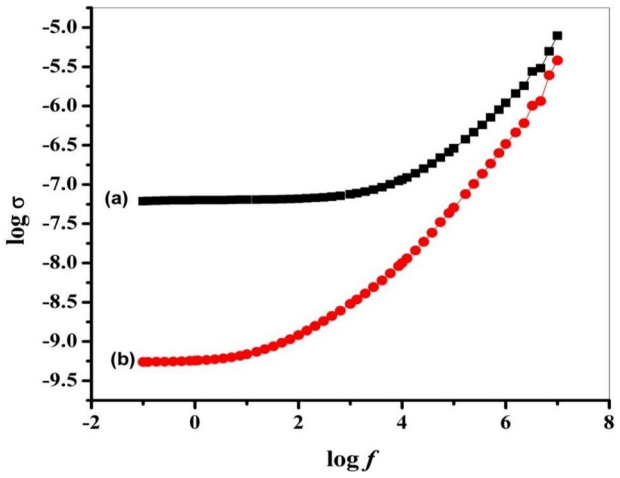

Fig. 10 Relation between log σ versus log f for **a** PAIFPA, and **b** PAIFPA-co-PSS

$$\sigma(\omega) = \sigma_{dc}(\omega) + \sigma ac(\omega) \quad (8)$$

As seen the conductivity of PAIFPA-co-PSS is lower than that for PAIFPA, and this attributed the decreasing of the mobility of free charge carrier and increasing the crystallinity of PAIFPA-co-PSS and this agreed with the results of XRD data and optical parameters.

Conclusion

The goal of this study is to create a novel poly((E)-2-((acryloyloxy)imino)-N-(4-fluorophenyl) acetamide) (PAIFPA) and its grafted structure with styrene sulfonate (PAIFPA-co-PSS). The chemical structure of the synthesized polymers was investigated by 1H NMR, FTIR, and XRD. The molecular weight of both PAIFPA, and PAIFPA-co-PSS was evaluated via 1H NMR analysis and found to be 8418, and 42,968, respectively. Further, the optical properties of PAIFPA, and PAIFPA-co-PSS was investigated where the absorbance was found to be in the blue shift and the bandgap was ranged from 2.6 eV to 3.5 Ev. and there is an increase in the band gap for PAIFPA-co-PSS is a short-wavelength light absorbers which can be used in tandem polymer solar cells. Eventually, the dielectric properties of PAIFPA and PAIFPA-co-PSS were performed, where PAIFPA-co-PSS shows electric conductivity values less than PAIFPA. This regarded to the generated electrostatic attraction between fluorine and sulfonate ion which leads to atoms rearrangement which results to increased crystallinity and this agreed to XRD.

Author Contributions The manuscript was written through contributions of all authors. All authors have given approval to the final version of the manuscript.

Funding Open access funding provided by The Science, Technology & Innovation Funding Authority (STDF) in cooperation with The Egyptian Knowledge Bank (EKB).

Declarations

Conflict of interest The authors declare there is no conflict of interest, financial, or otherwise.

References

1 Shirakawa H, Louis EJ, MacDiarmid AG, Chiang CK, Heeger AJ (1977) Synthesis of electrically conducting organic polymers: halogen derivatives of polyacetylene, (CH). J Chem Soc, Chem Commun 16:578–580
2 Zhao X, Zhan X (2011) Electron transporting semiconducting polymers in organic electronics. Chem Soc Rev 40(7):3728–3743
3 Nassar MA, Ward AA, Baseer RA (2013) Synthesis and characterization of polyaniline nanocomposites. KGK, Kaut Gummi Kunstst 66(9):39–46
4 Jabur AR (2018) Effect of polyaniline on the electrical conductivity and activation energy of electrospun nylon films. Int J Hydrogen Energy 43(1):530–536
5. Feast WJ (1986) Polyacetylene: Chemistry, physics, and material science. James C. W. Chien, Academic Press, Orlando, Florida, 1984. pp. xiv+634, price $89.00. ISBN 0–1 2- 172460–3. Br Polym J 18(3):209–209
6. Ehinger K, Summerfield S, Roth S (1985) Electrical conductivity of polyacetylene: nonsolitonic mechanism. Colloid Polym Sci 263(9):714–719
7. Baseer RA, Taha GM, Kassem AF, Khalil R (2020) Modified cotton fabrics with poly (3-(furan-2-carboamido) propionic acid) and poly (3-(furan-2-carboamido) propionic acid)/gelatin hydrogel for UV protection, antibacterial and electrical properties. Arab J Chem 13(6):5614–5626
8. Abbasi A, Bose A (2019) Massive and sustained enhancement of the electrical conductivity of polystyrene using multilayer graphene at Low loadings, and carbon black as a dispersion aid. Colloids Surf, A 580:123727
9. Arfin T, Mohammad F (2013) DC electrical conductivity of nanocomposite polystyrene–titanium–arsenate membrane. J Ind Eng Chem 19(6):2046–2051

10. Ahlatcıoğlu ÖE (2019) Electro-optical properties of poly (N-vinyl carbazole) nanoclay composites. Polym Bull 76(10):5301–5311
11. Okutan M, Yavuz E, Ahlatcıoğlu ÖE, Şenkal BF, Yalçın O, Yıldız A (2021) Impedance spectroscopy of polyaniline coated hydrogel. Polym Bull 78(8):4473–4486
12. Wang S, Wang L, Wang B, Su H, Fan W, Jing X (2021) Facile preparation of recyclable cyclic polyolefin/polystyrene vitrimers with low dielectric loss based on semi-interpenetrating polymer networks for high-frequency copper-clad laminates. Polymer 233:124214
13. Zhou Y, Fuentes-Hernandez C, Shim J, Meyer J, Giordano AJ, Li H, Winget P, Papadopoulos T, Cheun H, Kim J, Fenoll M, Dindar A, Haske W, Najafabadi E, Khan TM, Sojoudi H, Barlow S, Graham S, Brédas J-L, Marder SR, Kahn A, Kippelen B (2012) A Universal Method to Produce Low–Work Function Electrodes for Organic Electronics. Science 336(6079):327–332
14. Li Z, Qin F, Liu T, Ge R, Meng W, Tong J, Xiong S, Zhou Y (2015) Optical properties and conductivity of PEDOT:PSS films treated by polyethylenimine solution for organic solar cells. Org Electron 21:144–148
15. Reza KM, Gurung A, Bahrami B, Mabrouk S, Elbohy H, Pathak R, Chen K, Chowdhury AH, Rahman MT, Letourneau S, Yang H-C, Saianand G, Elam JW, Darling SB, Qiao Q (2020) Tailored PEDOT:PSS hole transport layer for higher performance in perovskite solar cells: Enhancement of electrical and optical properties with improved morphology. J Energy Chem 44:41–50
16. Xie C, Wang W, Li C, Nie Q, Sun L, Zeng W, Qin F, Liu T, Dong X, Han H, Fang H, Zhao D, Zhou Y (2021) Marangoni Force Assisted Spreading and Printing of Nanometer-Thick Polymer Films for Ubiquitous Optoelectronic Devices. Advanced Materials Technologies 6(7):2100181
17. Ouyang J, Chu C-W, Chen F-C, Xu Q, Yang Y (2005) High-Conductivity Poly(3,4-ethylenedioxythiophene):Poly(styrene sulfonate) Film and Its Application in Polymer Optoelectronic Devices. Adv Func Mater 15(2):203–208
18. Kraft A, Grimsdale AC, Holmes AB (1998) Electroluminescent Conjugated Polymers—Seeing Polymers in a New Light. Angew Chem Int Ed 37(4):402–428
19. Guo F, Xu R, Cui X, Zhang L, Wang K, Yao Y, Wei J (2016) High performance of stretchable carbon nanotube–polypyrrole fiber supercapacitors under dynamic deformation and temperature variation. Journal of Materials Chemistry A 4(23):9311–9318
20. Li P, Jin Z, Peng L, Zhao F, Xiao D, Jin Y, Yu G (2018) Stretchable All-Gel-State Fiber-Shaped Supercapacitors Enabled by Macromolecularly Interconnected 3D Graphene/Nanostructured Conductive Polymer Hydrogels. Adv Mater 30(18):1800124
21. Wang C, Yang M, Liu L, Xu Y, Zhang X, Cheng X, Gao S, Gao Y, Huo L (2020) One-step synthesis of polypyrrole/Fe2O3 nanocomposite and the enhanced response of NO2 at low temperature. J Colloid Interface Sci 560:312–320
22. Chen J, Yu Q, Cui X, Dong M, Zhang J, Wang C, Fan J, Zhu Y, Guo Z (2019) An overview of stretchable strain sensors from conductive polymer nanocomposites. Journal of Materials Chemistry C 7(38):11710–11730
23. Lv J, Zhou P, Zhang L, Zhong Y, Sui X, Wang B, Chen Z, Xu H, Mao Z (2019) High-performance textile electrodes for wearable electronics obtained by an improved in situ polymerization method. Chem Eng J 361:897–907
24. Oh JY, Rondeau-Gagné S, Chiu Y-C, Chortos A, Lissel F, Wang G-JN, Schroeder BC, Kurosawa T, Lopez J, Katsumata T, Xu J, Zhu C, Gu X, Bae W-G, Kim Y, Jin L, Chung JW, Tok JBH, Bao Z (2016) Intrinsically stretchable and healable semiconducting polymer for organic transistors. Nature 539(7629):411–415
25. Xu L, Cheng L, Wang C, Peng R, Liu Z (2014) Conjugated polymers for photothermal therapy of cancer. Polym Chem 5(5):1573–1580
26. Wang Y, Zhang H, Wang Z, Feng L (2020) Photothermal Conjugated Polymers and Their Biological Applications in Imaging and Therapy. ACS Applied Polymer Materials 2(10):4222–4240
27. Liang Y, Feng D, Wu Y, Tsai S-T, Li G, Ray C, Yu L (2009) Highly Efficient Solar Cell Polymers Developed via Fine-Tuning of Structural and Electronic Properties. J Am Chem Soc 131(22):7792–7799
28. Leclerc N, Chávez P, Ibraikulov OA, Heiser T, Lévêque P (2016) Impact of Backbone Fluorination on π-Conjugated Polymers in Organic Photovoltaic Devices: A Review. Polymers 8(1):11
29. Pérez G, Terraza CA, Coll D, Ortiz P, Aguilar-Vega M, González DM, Tagle LH, Tundidor-Camba A (2019) Synthesis and characterization of processable fluorinated aromatic poly(benzamide imide)s derived from cycloalkane substituted diamines, and their application in a computationally driven synthesis methodology. Polymer 162:121–129
30. Leivo E, Wilenius T, Kinos T, Vuoristo P, Mäntylä T (2004) Properties of thermally sprayed fluoropolymer PVDF, ECTFE, PFA and FEP coatings. Prog Org Coat 49(1):69–73
31. Kharitonov AP (2000) Practical applications of the direct fluorination of polymers. J Fluorine Chem 103(2):123–127
32. Kalia J, Raines RT (2008) Hydrolytic stability of hydrazones and oximes. Angew Chem Int Ed 47(39):7523–7526
33. Ritz J, Fuchs H, Kieczka H, Moran WC (2000) Caprolactam. Ullmann's Encyclopedia of Industrial Chemistry
34. Kassa J (2002) Review of oximes in the antidotal treatment of poisoning by organophosphorus nerve agents. J Toxicol Clin Toxicol 40(6):803–816
35. Panten J, Surburg H (2000) Flavors and fragrances, 2. Aliphatic compounds. Ullmann's Encyclopedia of Industrial Chemistry 1–55
36. Ulrich S, Boturyn D, Marra A, Renaudet O, Dumy P (2014) Oxime ligation: a chemoselective click-type reaction for accessing multifunctional biomolecular constructs. Chem A Eur J 20(1):34–41
37. Christman KL, Broyer RM, Tolstyka ZP, Maynard HD (2007) Site-specific protein immobilization through N-terminal oxime linkages. J Mater Chem 17(19):2021–2027
38. Sardesai VM, Waldshan TH (1991) Natural and synthetic intense sweeteners. J Nutr Biochem 2(5):236–244
39. Nicolau SE, Davis LL, Duncan CC, Olsen TR, Alexis F, Whitehead DC, Van Horn BA (2015) Oxime functionalization strategy for iodinated poly (epsilon-caprolactone) X-ray opaque materials. J Polym Sci, Part A: Polym Chem 53(20):2421–2430
40. Barrett DG, Yousaf MN (2008) Preparation of a class of versatile, chemoselective, and amorphous polyketoesters. Biomacromol 9(7):2029–2035
41. Liu J, Li RC, Sand GJ, Bulmus V, Davis TP, Maynard HD (2013) Keto-functionalized polymer scaffolds as versatile precursors to polymer side-chain conjugates. Macromolecules 46(1):8–14
42. Dhal PK, Polomoscanik SC, Gianolio DA, Starremans PG, Busch M, Alving K, Chen B, Miller RJ (2013) Well-defined aminooxy terminated N-(2-hydroxypropyl) methacrylamide macromers for site specific bioconjugation of glycoproteins. Bioconjug Chem 24(6):865–877
43. Heredia KL, Tolstyka ZP, Maynard HD (2007) Aminooxy end-functionalized polymers synthesized by ATRP for chemoselective conjugation to proteins. Macromolecules 40(14):4772–4779
44. Allaoua I, Goi BE, Obadia MM, Debuigne A, Detrembleur C, Drockenmuller E (2014) (Co) Polymerization of vinyl levulinate by cobalt-mediated radical polymerization and functionalization by ketoxime click chemistry. Polym Chem 5(8):2973–2979
45. Zhang L, You Z (2021) Dynamic Oxime-Urethane Bonds, a Versatile Unit of High Performance Self-healing Polymers for Diverse Applications. Chin J Polym Sci 39(10):1281–1291
46. He C, Shi S, Wang D, Helms BA, Russell TP (2019) Poly(oxime–ester) Vitrimers with Catalyst-Free Bond Exchange. J Am Chem Soc 141(35):13753–13757

47. Jang J, Ha J, Kim K (2008) Organic light-emitting diode with polyaniline-poly(styrene sulfonate) as a hole injection layer. Thin Solid Films 516(10):3152–3156
48. Al-Sabagh AM, Moustafa YM, Hamdy A, Killa HM, Ghanem RTM, Morsi RE (2018) Preparation and characterization of sulfonated polystyrene/magnetite nanocomposites for organic dye adsorption. Egypt J Pet 27(3):403–413
49. Jin YH, Kim J, Im SS (2004) Synthesis and characterization of ω-sulfonated polystyrene-stabilized cadmium sulfide nanoclusters. Macromol Res 12(6):604–607
50. Beccari MV, Meaney CJ (2017) Clinical utility of patiromer, sodium zirconium cyclosilicate, and sodium polystyrene sulfonate for the treatment of hyperkalemia: an evidence-based review. Core evidence 12:11
51. Wibowo FR, Saputra OA, Lestari WW, Koketsu M, Mukti RR, Martien R (2020) pH-triggered drug release controlled by poly (styrene sulfonate) growth hollow mesoporous silica nanoparticles. ACS Omega 5(8):4261–4269
52. McGowan C, Saha S, Chu G, Resnick M, Moss S (2009) Intestinal necrosis due to sodium polystyrene sulfonate (Kayexalate) in sorbitol. South Med J 102(5):493
53. Sandmeyer T (1919) Isatin synthesis. Helv Chim Acta 2(1):234–238
54. Klein DR (2020) Organic chemistry. John Wiley & Sons
55. Vandenbergh J, Junkers T, Olabisi O, Adewale K (2016) Polyacrylates. Handbook of Thermoplastics 2
56. Inaba M, Ando M, Hatanaka A, Nomoto A, Matsuzawa K, Tasaka A, Kinumoto T, Iriyama Y, Ogumi Z (2006) Controlled growth and shape formation of platinum nanoparticles and their electrochemical properties. Electrochim Acta 52(4):1632–1638
57. Barth HG, Mays JW (1991) Modern methods of polymer characterization. Vol. 115. John Wiley & Sons
58. Izunobi JU, Higginbotham CL (2011) Polymer Molecular Weight Analysis by 1H NMR Spectroscopy. J Chem Educ 88(8):1098–1104
59. Vasquez ES, Cunningham JL, McMahan JB, Simpson CL, Walters KB (2015) Fetuin-A adsorption and stabilization of calcium carbonate nanoparticles in a simulated body fluid. Journal of Materials Chemistry B 3(31):6411–6419
60. Yao SF, Chen XT, Ye HM (2017) Investigation of Structure and Crystallization Behavior of Poly(butylene succinate) by Fourier Transform Infrared Spectroscopy. J Phys Chem B 121(40):9476–9485
61 Kovacic JE (1967) The C N stretching frequency in the infrared spectra of Schiff's base complexes—I. Copper complexes of salicylidene anilines. Spectrochim Acta A Mol Spectrosc 23(1):183–187
62. Zhuang J, Li M, Pu Y, Ragauskas AJ, Yoo CG (2020) Observation of Potential Contaminants in Processed Biomass Using Fourier Transform Infrared Spectroscopy. Appl Sci 10(12):4345
63. Dave N, Troullier A, Mus-Veteau I, Duñach M, Leblanc G, Padrós E (2000) Secondary structure components and properties of the melibiose permease from Escherichia coli: a fourier transform infrared spectroscopy analysis. Biophys J 79(2):747–755
64. Heredia-Guerrero JA, Benítez JJ, Domínguez E, Bayer IS, Cingolani R, Athanassiou A, Heredia A (2014) Infrared and Raman spectroscopic features of plant cuticles: a review. Front Plant Sci 5(305)
65. Rashid T, Kait CF, Murugesan T (2016) A "Fourier Transformed Infrared" Compound Study of Lignin Recovered from a Formic Acid Process. Procedia Engineering 148:1312–1319
66. Ramasamy R (2014) FTIR and FT-RAMAN Spectral Investigation of Fluorobenzene. International Journal of Physics and Applications 6(1):1–6
67. Nabid MR, Entezami AA (2004) A novel method for synthesis of water-soluble polypyrrole with horseradish peroxidase enzyme. J Appl Polym Sci 94(1):254–258
68. Alemu D, Wei H-Y, Ho K-C, Chu C-W (2012) Highly conductive PEDOT:PSS electrode by simple film treatment with methanol for ITO-free polymer solar cells. Energy Environ Sci 5(11):9662–9671
69. Kumar SCS, Kumar NV, Srinivas P, Bettadaiah BK (2014) A convenient practical synthesis of alkyl and aryl oxime esters. Synthesis 46(14):1847–1852
70. Behniafar H, Sedaghatdoost M (2011) New fluorinated aromatic poly(ether-amide)s derived from 2,2′-bis(3,4,5-trifluorophenyl)-4,4′-diaminodiphenyl ether and various dicarboxylic acids. J Fluorine Chem 132(4):276–284
71. Sultan M, Nagieb ZA, El-Masry HM, Taha GM (2021) Physically-crosslinked hydroxyethyl cellulose-g-poly (acrylic acid-co-acrylamide)-Fe3+/silver nanoparticles for water disinfection and enhanced adsorption of basic methylene blue dye. Int J Biol Macromol
72. Mehrdad A, Parvini E (2019) Interactions of sodium polystyrene sulfonate with 4-methylpyridinium based ionic liquids in aqueous solution: Viscometry, conductometry, UV–Vis spectroscopy and density functional theory studies. J Chem Thermodyn 131:503–516
73. Tauc J, Menth A, Wood DL (1970) Optical and Magnetic Investigations of the Localized States in Semiconducting Glasses. Phys Rev Lett 25(11):749–752
74. Shportko K (2019) Disorder and compositional dependences in Urbach-Martienssen tails in amorphous (GeTe) x (Sb 2 Te 3) 1–x alloys. Sci Rep 9(1):1–9
75. Park YW (2010) Editorial for the Conducting Polymers for Carbon Electronics themed issue. Chem Soc Rev 39(7):2352–2353
76. Assad H, Kharroubi M (2021) Dielectric studies and Cole-Cole plot analysis of Na2O–(1–x) ZnO–xCoO–P2O5 glasses. J Non-Cryst Solids 560:120721
77. Rozik NN, Khalaf AI, Ward AA (2016) Studies the behaviors of polyaniline on the properties of PS/PMMA blends. Proceedings of the Institution of Mechanical Engineers, Part L: Journal of Materials: Design and Applications 230(2):526–536
78. Gad SA, Moustafa AM, Ward AA (2015) Preparation and Some Physical Properties of Zn1−xCrxO. J Inorg Organomet Polym Mater 25(5):1077–1087
79. Hassan ML, Fadel SM, Ward AA, Moorefield CM, Newkome GR (2016) Electrical properties of FeII-terpyridine-Modified cellulose nanocrystals and polycaprolactone/FeII-CTP nanocomposites. Polym Compos 37(9):2734–2743